PERGAMON

International Journal of Heat and Mass Transfer 45 (2002) 3973–3985

International Journal of HEAT and MASS TRANSFER

www.elsevier.com/locate/ijhmt

Analysis of three-dimensional heat transfer in micro-channel heat sinks

Weilin Qu, Issam Mudawar *

Boiling and Two-phase Flow Laboratory, School of Mechanical Engineering, Purdue University, West Lafayette, IN 47907, USA

Received 12 January 2001; received in revised form 23 February 2002

Abstract

In this study, the three-dimensional fluid flow and heat transfer in a rectangular micro-channel heat sink are analyzed numerically using water as the cooling fluid. The heat sink consists of a 1-cm^2 silicon wafer. The micro-channels have a width of 57 μm and a depth of 180 μm, and are separated by a 43 μm wall. A numerical code based on the finite difference method and the SIMPLE algorithm is developed to solve the governing equations. The code is carefully validated by comparing the predictions with analytical solutions and available experimental data. For the micro-channel heat sink investigated, it is found that the temperature rise along the flow direction in the solid and fluid regions can be approximated as linear. The highest temperature is encountered at the heated base surface of the heat sink immediately above the channel outlet. The heat flux and Nusselt number have much higher values near the channel inlet and vary around the channel periphery, approaching zero in the corners. Flow Reynolds number affects the length of the flow developing region. For a relatively high Reynolds number of 1400, fully developed flow may not be achieved inside the heat sink. Increasing the thermal conductivity of the solid substrate reduces the temperature at the heated base surface of the heat sink, especially near the channel outlet. Although the classical fin analysis method provides a simplified means to modeling heat transfer in micro-channel heat sinks, some key assumptions introduced in the fin method deviate significantly from the real situation, which may compromise the accuracy of this method.

1. Introduction

Advanced very large-scale integration (VLSI) technology has resulted in significant improvements in the performance of electronic systems in the past decades. With the trend toward higher circuit density and faster operation speed, however, there is a steady increase in the dissipative heat flux at the component, module, and system levels. It has been shown that most operation parameters of an electronic component are strongly affected by its temperature as well as its immediate thermal environment. This leads to an increasing demand for highly efficient electronic cooling technologies. To meet this demand, various electronic cooling schemes have been developed. Comprehensive reviews of the different heat transfer techniques employed in electronic cooling were provided by Mudawar [1] and Yeh [2].

Among others, the micro-channel heat sink has been proven to be a high performance cooling method. A schematic of the structure of a rectangular micro-channel heat sink is illustrated in Fig. 1. A large number of flow channels with characteristic dimensions ranging from 10 to 1000 μm are fabricated in a solid substrate which usually has high thermal conductivity such as silicon or copper. An electronic component is then mounted on the base surface of the heat sink. The heat generated by the component is first transferred to the channels by heat conduction through the solid, and removed by the cooling fluid which is forced to flow through the channels.

The micro-channel heat sink combines the attributes of high surface area per unit volume, large heat transfer

* Corresponding author. Tel.: +1-765-494-5705; fax: +1-765-494-0539.

E-mail address: mudawar@ecn.purdue.edu (I. Mudawar).

0017-9310/02/$ - see front matter
PII: S0017-9310(02)00101-1

Nomenclature

A_c	cross-sectional area of channel
C_f	friction coefficient
c_p	specific heat at constant pressure
d_h	hydraulic diameter of channel, that is, four times ratio of cross-sectional area to wetted perimeter
f	friction factor
H	height of micro-channel heat sink
H_{ch}	height of micro-channel
H_{w1}	substrate thickness on insulated side of micro-channel heat sink
H_{w2}	substrate thickness on heated side of micro-channel heat sink
i	number of iteration
k	thermal conductivity
L	length of micro-channel heat sink
n	outer normal coordinate at interface between the solid and fluid
Nu	Nusselt number
P	pressure
q''	heat flux
Re	Reynolds number based on channel hydraulic diameter
R_t	thermal resistance
T	temperature
T_{in}	fluid inlet temperature
T_m	fluid bulk temperature
u, v, w	velocity component in the x, y, z direction respectively
$\vec{V}$	velocity vector
W	width of micro-channel heat sink unit cell
W_{ch}	width of micro-channel
W_{w1}, W_{w2}	half-thickness of wall separating micro-channels
x, y, z	Cartesian coordinates

Greek symbols

μ	dynamic viscosity
ρ	density

Subscripts

av	average
f	fluid
in	inlet
s	solid
w	heat sink top wall
Γ	interface between the solid and fluid

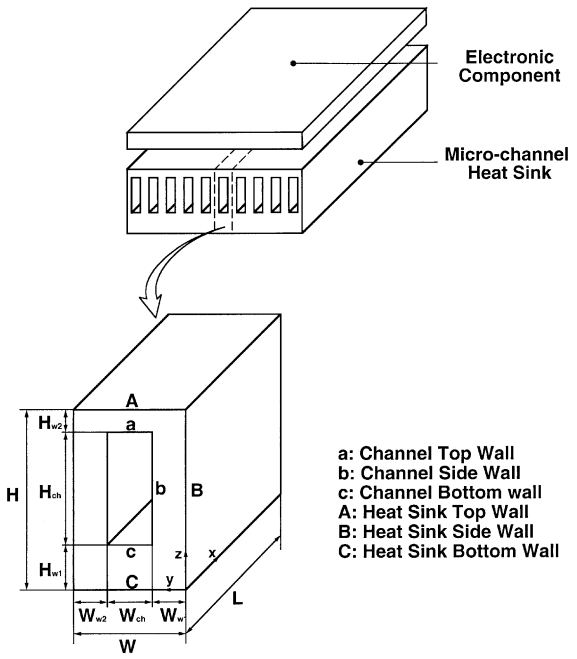

Fig. 1. Schematic of rectangular micro-channel heat sink and unit cell.

coefficient, and small cooling fluid inventory. Its inherent advantages attracted considerable attentions from researchers. Micro-channel heat sinks with various designs and cooling fluids were fabricated and tested, and superiority of this novel cooling technique was confirmed by experimental results [3–9]. Tuckerman and Pease [3] fabricated a micro-channel heat sink by chemically etching parallel channels in a 1-cm^2 silicon wafer. The channels had a width of 50 μm and a depth of 302 μm, and were separated by 50 μm thick walls. Using water as cooling fluid, Tuckerman and Pease [3] demonstrated that their micro-channel heat sink was capable of dissipating a heat flux of 790 W/cm^2. Mudawar and Bowers [4] employed a stainless steel micro-tube in their heat transfer experiments. The micro-tube had an inner diameter of 902 μm, wall thickness of 89 μm and length of 5.8 mm. They demonstrated heat fluxes as high as 3000 W/cm^2 for single-phase water flow.

In addition to the experimental work, many analytical studies on heat transfer in micro-channel heat sinks are found in the literature [10–18]. The classical fin analysis method was widely adopted in these studies. Basically, the solid region separating two flow channels is approximated as a thin fin. The results from the classical fin analysis are then directly applied to model the heat transfer process in micro-channel heat sinks. This method provides a simplified means to evaluating the global heat transfer characteristics. However, it should be noted that a number of major assumptions are

usually employed. Some of them may deviate significantly from the real situation, which will reduce the accuracy of the analytical model.

Wesberg et al. [15] provided a more realistic picture by solving numerically a two-dimensional conjugate heat transfer problem which consists of the simultaneous calculation of heat conduction in the solid and convective heat transfer in the fluid. Detailed spatial distributions of temperature, heat flux and Nusselt number along a micro-channel heat sink cross-section were obtained. A major assumption introduced by Wesberg et al. [15] was that the flow is fully developed (hydraulically and thermally). More recently, Fedorov and Viskanta [18] developed a three-dimensional model to investigate the conjugate heat transfer in a micro-channel heat sink. The approximation of fully developed flow was eliminated and the development of the velocity and temperature field was considered. A very complex yet unusual heat transfer pattern was obtained due to the combined convection–conduction effects in the three-dimensional setting. Most noticeable is that the average channel wall temperature along the flow direction was nearly uniform except in the region close to the channel inlet, where a very large temperature gradient was found. However, most studies in this field reported that the wall temperature rise along the flow direction is nearly linear [12–15,17].

Although micro-channel heat sinks are capable of dissipating high heat fluxes, the small flow rate produces a large temperature rise along the flow direction in both the solid and cooling fluid, which can be damaging to the temperature sensitive electronic components. Therefore, more sophisticated predictions of the temperature field are essential for an effective micro-channel heat sink design. A more accurate description of the heat transfer characteristics can only be obtained by direct numerical simulation of three-dimensional fluid flow and heat transfer in both the solid and cooling fluid.

In this study, a numerical analysis is performed for the transport processes in a rectangular micro-channel heat sink. The Navier–Stokes and energy equations are solved numerically to determine the fluid flow and heat transfer characteristics of the heat sink. It should be noted here that several previous experimental observations found that the fluid flow and heat transfer in micro-channels may behave differently from those in macroscale channels [19–23]. In particular, Choi et al. [19] and Yu et al. [20] studied fluid flow and heat transfer characteristics of nitrogen gas and water in micro-tubes with inner diameter ranging from 3 to 102 μm. They reported that the measured friction factors were less than predictions from the macroscale tube correlations, and the measured Nusselt numbers were larger than predictions from the Dittus–Boelter correlation. Peng and Peterson [21] investigated the single-phase forced convective heat transfer of water in rectangular channels with hydraulic diameter ranging from 133 to 367 μm. Their results indicted that the Reynolds number for transition from laminar to turbulent flow became much smaller than in the macroscale channels, and the aspect ratio of the channel had a significant effect on the convective heat transfer. Mala and Li [23] measured pressure gradients of water flow in micro-tubes with inner diameter ranging from 50 to 254 μm. They found for larger micro-tubes with inner diameter above 150 μm, the experimental results were in rough agreement with the conventional theory. For smaller micro-tubes, the pressure gradients were higher than these predicted by the conventional theory. Furthermore, the differences between the experimental results and conventional theory predictions increased with increasing Reynolds number. Few attempts have been made to provide theoretical explanations for these fluid flow and heat transfer behaviors in micro-channels. For gas flow, Pong et al. [24] attributed some of these trends to breakdown of the continuum assumptions when the channel size was close to the mean free path of the gas medium, i.e., in the order of magnitude of 1 μm. The other possible explanation was the compressibility due to the high pressure loss. Liquid on the other hand is more complicated, and so far no widely accepted theoretical explanation for liquid flow in micro-channels can be found from the literature. It is clear that an effective analysis of micro-channel heat sinks requires a fundamental understanding of the fluid flow and heat transfer characteristics in such micro-channels. However, due to inconsistencies between experimental results and the lack of understanding of the underlying phenomena, the classical Navier–Stokes and energy equations are used in the present study.

Based on the numerical results, a detailed description of the local and average heat transfer characteristics, i.e. temperature, heat flux, and Nusselt number, is given, and the effects of flow Reynolds number and thermal conductivity of the solid substrate on the heat transfer process are discussed. The results provide a fundamental insight into the complicated three-dimensional heat transfer pattern and may be utilized as a basis to verify the classical fin analysis method.

2. Numerical analysis

2.1. Governing equations and boundary conditions

The construction of the micro-channel heat sink employed to perform the numerical analysis is chosen to match the one used in Kawano et al.'s experimental work [9]. The structure of the heat sink is illustrated in Fig. 1. The heat sink is made from silicon and water is used as the cooling fluid. The electronic component is

idealized as a constant heat flux boundary condition at the heat sink top wall.

Taking advantage of symmetry, a unit cell consisting of only one channel and the surrounding solid is chosen as shown by the dashed lines in Fig. 1. Attention is focused on the heat transfer process in a single unit cell. The results obtained can be easily extended to the entire heat sink. Fig. 1 shows the unit cell, the corresponding coordinate system, and some important notations. Dimensions of the heat sink unit cell are given in Table 1.

Heat transport in the unit cell is a conjugate problem which combines heat conduction in the solid and convective heat transfer to the cooling fluid. The two heat transfer modes are coupled by the continuities of temperature and heat flux at the interface between the solid and fluid, which are expressed as

$$T_{s,\Gamma} = T_{f,\Gamma}, \tag{1}$$

$$-k_s \left.\frac{\partial T_s}{\partial n}\right|_{\Gamma} = -k_f \left.\frac{\partial T_f}{\partial n}\right|_{\Gamma}. \tag{2}$$

Some simplifying assumptions are required before applying the conventional Navier–Stokes and energy equations to model the heat transfer process in the heat sink. The major assumptions are:

(1) steady fluid flow and heat transfer,
(2) incompressible fluid,
(3) laminar flow,
(4) constant solid and fluid properties,
(5) negligible radiation heat transfer,
(6) negligible superimposed natural convective heat transfer.

Based on these approximations, the governing differential equations used to describe the fluid flow and heat transfer in the heat sink unit cell are established. First consider the cooling fluid. The momentum equation is written as

$$\rho_f\left(\vec{V}\cdot\nabla\vec{V}\right) = -\nabla P + \mu_f\nabla^2\vec{V}, \tag{3}$$

and the energy equation is

$$\rho_f c_{p,f}\left(\vec{V}\cdot\nabla T\right) = k_f\nabla^2 T. \tag{4}$$

For the solid, the momentum equation is simply

$$\vec{V} = \vec{0}, \tag{5}$$

Table 1
Dimensions of unit cell of micro-channel heat sink

W_{w1} (μm)	W_{ch} (μm)	W_{w2} (μm)	H_{w1} (μm)	H_{ch} (μm)	H_{w2} (μm)	L (mm)
21.5	57	21.5	270	180	450	10

and the energy equation is

$$k_s\nabla^2 T = 0. \tag{6}$$

If the whole unit cell is chosen as a unitary domain, the boundary conditions can be specified as follows. For the hydraulic boundary conditions, the velocity is zero at all boundaries except the channel inlet and outlet. A uniform velocity is applied at the channel inlet.

$$u = \frac{Re\cdot\mu_f}{d_h},\ v = 0,\ w = 0,$$
$$\text{for } x = 0,\ W_{w1} \leqslant y \leqslant W_{w1} + W_{ch},\ \text{and}$$
$$H_{w1} \leqslant z \leqslant H_{w1} + H_{ch}. \tag{7}$$

The flow is fully developed at the channel outlet.

$$\frac{\partial u}{\partial x} = 0,\ \frac{\partial v}{\partial x} = 0,\ \frac{\partial w}{\partial x} = 0,$$
$$\text{for } x = L,\ W_{w1} \leqslant y \leqslant W_{w1} + W_{ch},\ \text{and}$$
$$H_{w1} \leqslant z \leqslant H_{w1} + H_{ch}. \tag{8}$$

For the thermal boundary conditions, adiabatic boundary conditions are applied to all the boundaries of the solid region except the heat sink top wall, where a constant heat flux is assumed.

$$-k_s\frac{\partial T}{\partial z} = q'', \quad \text{for } 0 \leqslant x \leqslant L,\ 0 \leqslant y \leqslant W,\ \text{and } z = H. \tag{9}$$

At the channel inlet, the liquid temperature is equal to a given constant inlet temperature.

$$T = T_{in}, \quad \text{for } x = 0,\ W_{w1} \leqslant y \leqslant W_{w1} + W_{ch},$$
$$\text{and } H_{w1} \leqslant z \leqslant H_{w1} + H_{ch}. \tag{10}$$

The flow is assumed thermally fully developed at the channel outlet.

$$\frac{\partial^2 T}{\partial x^2} = 0, \qquad \text{for } x = L,\ W_{w1} \leqslant y \leqslant W_{w1} + W_{ch},$$
$$\text{and } H_{w1} \leqslant z \leqslant H_{w1} + H_{ch}. \tag{11}$$

It should be noted here that the temperature field may not be fully developed if the entrance length is longer than the channel length, as demonstrated later in this paper. However, the change of temperature gradient along the flow direction at the channel exit is usually very small even for very large Reynolds numbers. Therefore, using Eq. (11) as the exit thermal boundary condition will not introduce a large numerical error.

2.2. Method of solution

The finite difference method and the SIMPLE algorithm [25] are applied to solve the governing differential

equations. The grid system has 120 nodes in the x-direction, 30 nodes in the y-direction and 50 nodes in the z-direction. A non-uniform grid arrangement in the x-direction with a large number of grid points near the channel inlet is used to resolve the flow developing region. The resulting system of algebraic equations is solved using the Gauss–Seidal iterative technique, with successive over-relaxation to improve the convergence time. The solution is regarded as convergent when the criterion of $\max|(\phi^{i+1}-\phi^{i})/\phi^{i+1}| \leqslant 10^{-6}$ is satisfied, where ϕ represents any dependent variable, namely u, v, w, and T, and i is the number of iteration.

Some special numerical techniques are required when applying the finite difference method to a conjugate heat transfer problem, which were discussed in details by Patankar [25,26]. Basically, the whole heat transfer unit cell is chosen as a unitary computation domain. The momentum equation is solved in a usual manner by assigning the true value to the viscosity in the fluid and a very large value to the viscosity in the solid. In this way, if a zero velocity is specified as the boundary condition for the solid region, the high viscosity in the solid will establish a zero velocity throughout the solid phase, thus provide the appropriate no-slip boundary condition to the fluid region. Once the velocity field is determined, the energy equation can be solved after specifying the thermal conductivities for the solid and fluid.

2.3. Code validation

The numerical code is verified in a number of ways to ensure the validity of the numerical analysis. The grid dependence test is first conducted by using several different mesh sizes. This test proved that the results based on the final grid system presented in this paper are independent of mesh size.

The numerical code is then evaluated by comparing the results with available analytical solutions or widely accepted numerical results. Fig. 2 shows a dimensionless velocity profile for fully developed flow in the channel. The dimensionless velocity here is defined as $u/u_{\max}$, where $u_{\max}$ is the maximum velocity located at the center of the rectangular channel. Excellent agreement is found between the present numerical prediction and the analytical solution [27]. For comparison, the analytical and numerical velocity profiles at the z middle plan ($z = H_{\mathrm{w1}} + H_{\mathrm{ch}}/2$) and y middle plane ($y = W_{\mathrm{w1}} + W_{\mathrm{ch}}/2$) are plotted in Fig. 1. The difference is so small that the two results are virtually identical.

The solution for the energy equation was also verified. The surrounding solid region is removed and a pure convective heat transfer problem in the rectangular channel is considered. The boundary condition is chosen as constant longitudinal wall heat flux with uniform peripheral heat flux. Based on the numerical results, the average peripheral Nusselt number $\overline{Nu}$ is evaluated and

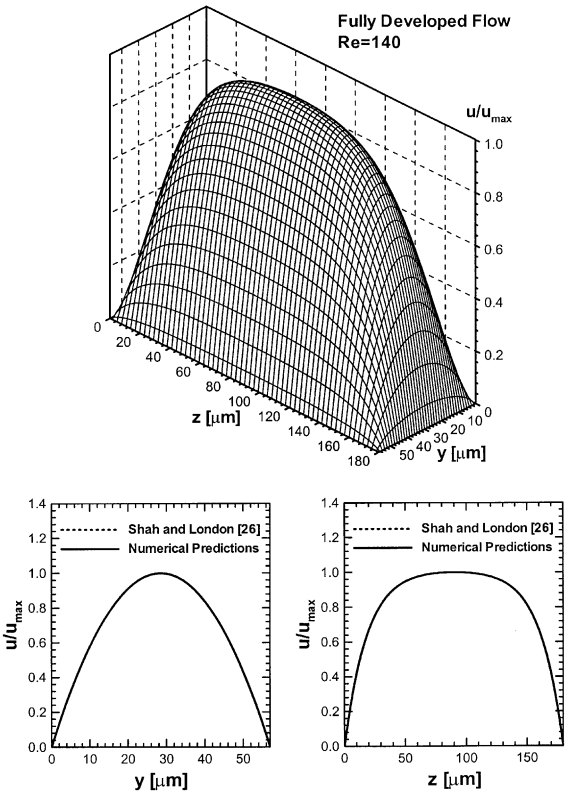

Fig. 2. Comparison between numerical predictions and analytical solution for fully developed velocity profile in a rectangular channel.

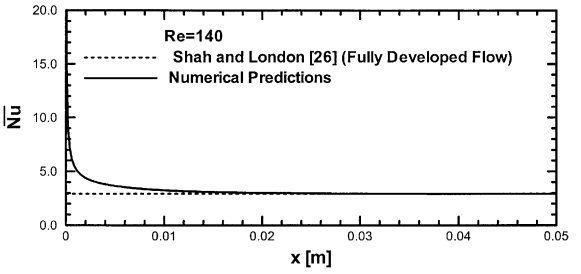

Fig. 3. Comparison between numerical predictions and analytical solution for average Nusselt number in a rectangular channel.

plotted in Fig. 3 as a function of the longitudinal distance x. $\overline{Nu}$ is defined as

$$\overline{Nu} = \frac{q'' d_{\mathrm{h}}}{k_{\mathrm{f}}(T_{\Gamma,\mathrm{m}} - T_{\mathrm{m}})}, \tag{12}$$

where $T_{\Gamma,\mathrm{m}}$ is the average temperature at the boundary

$$T_{\Gamma,\mathrm{m}} = \frac{1}{\Gamma}\int_{\Gamma} T_{\Gamma}\,\mathrm{d}\Gamma, \tag{13}$$

and T_m is the fluid bulk temperature.

$$T_m = \frac{\int_{A_c} uT \, dA_c}{\int_{A_c} u \, dA_c}. \quad (14)$$

This is a classical convective heat transfer problem and a solution for fully developed flow was provided by Shah and London [27], which is also plotted in Fig. 3. Fig. 3 shows that $\overline{Nu}$ is high in the entrance region, but quickly approaches the fully developed value.

In addition to the comparison with the theoretical results, the present numerical results were also compared with experimental data by Kawano et al. [9]. Fig. 4 compares the numerically predicted and experimentally measured friction coefficient, C_f, inlet thermal resistance, $R_{t,in}$, and outlet thermal resistance, $R_{t,out}$, for a wide range of Reynolds numbers. These parameters are defined, respectively, as

$$C_f = f \cdot Re, \quad (15)$$

$$R_{t,in} = \frac{T_{w,in} - T_{in}}{q''}, \quad (16)$$

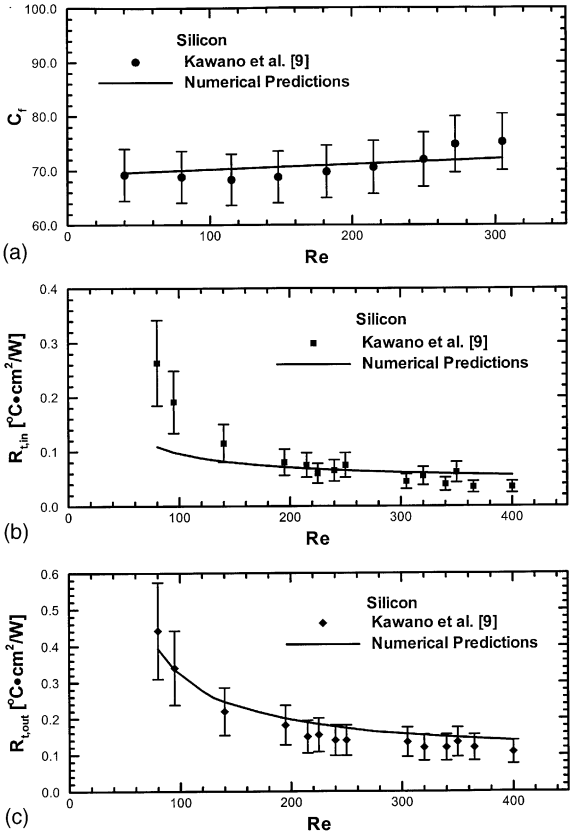

Fig. 4. Comparison between numerical predictions and experimental data for (a) friction coefficient, (b) inlet thermal resistance, and (c) outlet thermal resistance.

$$R_{t,out} = \frac{T_{w,out} - T_{in}}{q''}. \quad (17)$$

Fig. 4 shows good agreement between the present numerical predictions and the experimental data. Most of the predicted results lie within the range of experimental uncertainties, which are outlined by error bars. The only exception is the inlet thermal resistance, $R_{t,in}$, at lower Reynolds numbers, where the numerical results appear to be underpredicted. A possible explanation for this underprediction may be the heat loss during the experiments. Some heat would spread into the upstream plenum of the solid substrate and be dissipated to the ambiant. This would reduce the effective heat flux q'' resulting in a larger measured thermal resistance as indicated in Eq. (16). This effect should be more significant for small Reynolds numbers where the convective heat transfer to the cooling liquid is generally weak. Additionally, Kawano et al. indicated these low Reynolds number conditions were unreliable because of large temperature-induced viscosity gradients at the inlet portion [9].

The above code verification tests provide confidence in the present numerical method. A detailed discussion of the parametric trends of the numerical study follows.

3. Results and discussion

The numerical analysis was performed for the rectangular micro-channel heat sink and the results are presented in this section. Some important fluid flow and heat transfer parameters that are employed in this study are summarized in Table 2. The local and average heat transfer characteristics of the heat sink are explored first. Then the effects of flow Reynolds number and thermal conductivity of the solid are discussed. Finally, the validity of some major assumptions employed in the classical fin analysis method is assessed.

3.1. Local heat transfer characteristics

The temperature distribution at several x–y planes, namely the heat sink top wall (wall A), channel top wall (wall a), channel bottom wall (wall c), and heat sink bottom wall (wall C), is illustrated in Fig. 5a–d. Some interesting features are readily observed. From the distribution of constant temperature contour lines, the

Table 2
Fluid flow and heat transfer parameters employed in numerical analysis

Re	T_{in} (°C)	q'' (W/cm²)	k_{water} (W/m °C)	$k_{silicon}$ (W/m °C)	k_{copper} (W/m °C)
140.0	20.0	90.0	0.61	148.0	401.0

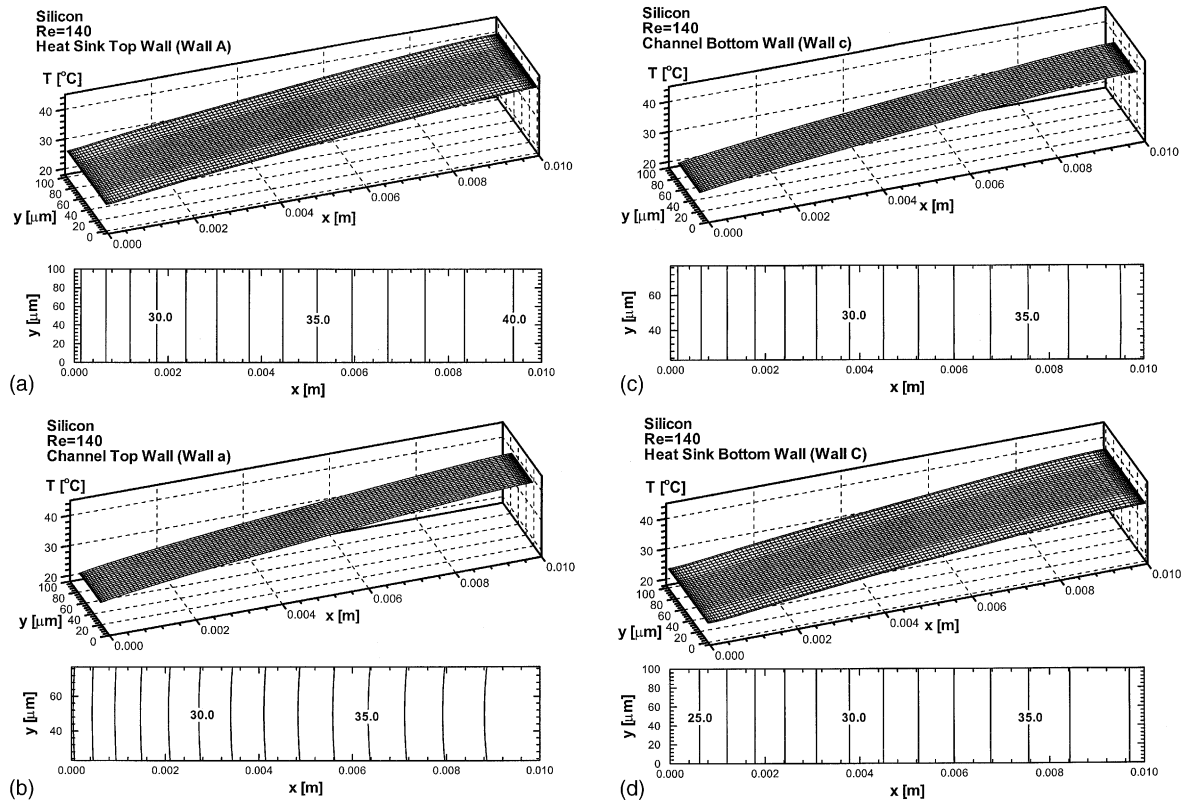

Fig. 5. Local temperature distribution in x–y plane: (a) heat sink top wall (wall A), (b) channel top wall (wall a), (c) channel bottom wall (wall c), (d) heat sink bottom wall (wall C).

temperature gradient decreases along the longitudinal x-direction from the channel inlet to the outlet. However, the change of gradient is so small that a linear temperature rise is a good approximation for the situation studied. The temperature along the transverse y-direction is virtually constant. The temperature decreases from the heat sink top wall to the heat sink bottom wall.

The temperature distributions at two x–z planes, the y middle plane where $y = W_{w1} + W_{ch}/2$ and the heat sink side wall (wall B), are plotted in Fig. 6a and b, respectively. In Fig. 6a, the shape of the channel is clearly visible due to the large difference in temperature gradient between the solid and liquid. Because of the silicon's high thermal conductivity, the temperature gradient in the silicon is much smaller than that in water. The location of the channel is noted in Fig. 6b. The positions of the constant temperature contour lines are essentially the same in the solid region in Fig. 6a and b, which confirms that the temperature is nearly constant along the transverse y-direction in the solid. It can also be seen from Fig. 6a and b that the temperature gradient along the z-direction in the solid region above the channel is larger than that in the solid region below the channel at a given longitudinal distance x. In fact, the temperature gradient in the solid region below the channel is so small that it can be regarded as isothermal at each y–z cross-section. This implies that the thickness and material in the solid region above the channel are more important for heat transport in the heat sink.

Fig. 7a–c show temperature distributions at three y–z cross-sections along longitudinal x-direction, where $x = 0$, $x = L/2$ and $x = L$. The temperature variation in the solid is much smaller than in the fluid. The temperature of the fluid is originally uniform at the channel inlet ($x = 0$) and changes due to the development of the thermal boundary layer. The temperature profile at the middle of the channel ($x = L/2$) is very close to that at the channel exit ($x = L$).

Fig. 8a–c illustrate the heat flux distribution at the channel walls. The local heat flux q'' is evaluated as

$$q'' = -k_s \left.\frac{\partial T_s}{\partial n}\right|_{\Gamma}. \tag{18}$$

A high heat flux is found in the region near the channel inlet. This is attributed to the thin thermal boundary layer in the developing region. The heat flux varies around the channel periphery, approaching zero in the corners where the flow is generally weak for a

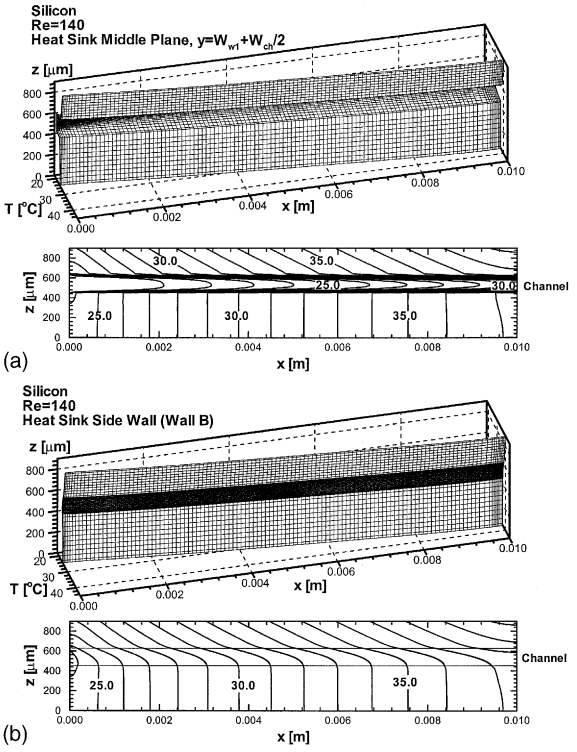

Fig. 6. Local temperature distribution in x–z plane: (a) heat sink middle plane ($y = W_{w1} + W_{ch}/2$), (b) heat sink side wall (wall B).

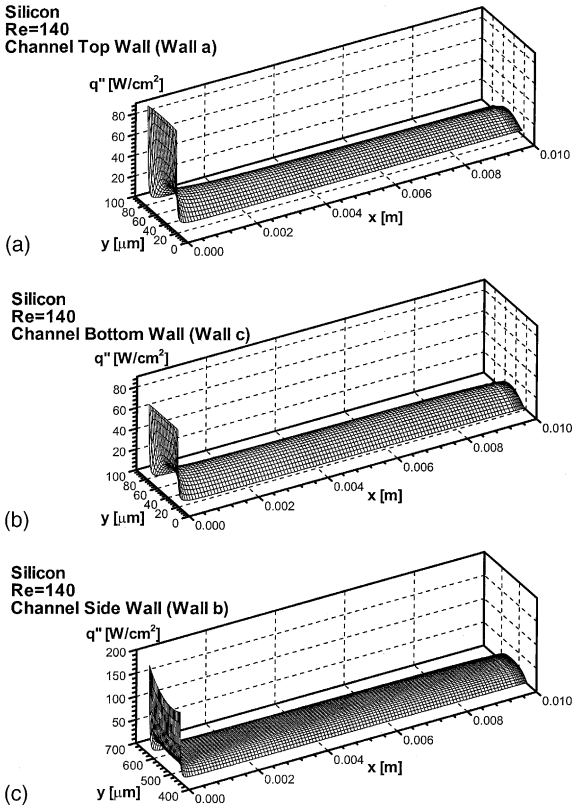

Fig. 8. Local heat flux distribution: (a) channel top wall (wall a), (b) channel bottom wall (wall c), (c) channel side wall (wall b).

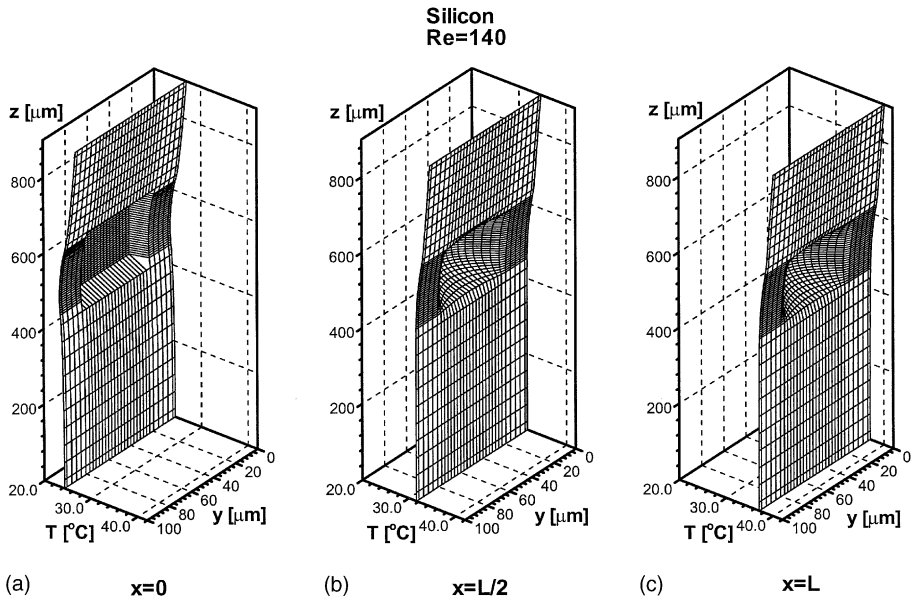

Fig. 7. Local temperature distribution in y–z plane: (a) heat sink inlet ($x = 0$), (b) heat sink middle plane ($x = L/2$), (c) heat sink outlet ($x = L$).

rectangular channel. Comparing Fig. 8a with b, the heat flux at the channel top wall is only slightly larger than that at the bottom wall. This implies that although the heat is supplied to the heat sink top wall, it is spread out very effectively within the solid region by conduction. From Fig. 8c, the heat flux at the channel side wall is higher than that at the channel top and bottom walls due to the short distance between the channel side walls and the large velocity gradient present.

The heat flux distribution can be better understood from the local Nusselt number distribution at the corresponding three channel walls, which are shown in Fig. 9a–c. The local Nusselt number Nu is defined as

$$Nu = \frac{q'' d_h}{k_f(T_{s,\Gamma} - T_m)}, \tag{19}$$

where T_m is the fluid bulk temperature defined by Eq. (13). Some features of the Nusselt number distribution are the same as those in the heat flux distribution, such as high value in the entrance region and low value near the channel corners. There are also some special features. The Nusselt number distributions at the channel top and bottom walls are essentially identical. The Nusselt number at the side wall is symmetrical about the middle plane, which is different from the corresponding heat flux distribution. This is because for laminar flow with constant properties, the Nusselt number is solely determined by the channel geometry and local flow conditions.

3.2. Bulk heat transfer characteristics

The fluid bulk temperature and average wall temperatures at the heat sink top wall, channel top wall, channel bottom wall, and heat sink bottom wall are plotted in Fig. 10a as functions of longitudinal distance x. The fluid bulk temperature T_m is defined in Eq. (3). The average wall temperature at the heat sink top wall (wall A) and heat sink bottom wall (wall C) is defined as

$$T_{av}(x) = \frac{1}{W}\int_0^W T_{s,\Gamma}\,dy, \quad \text{for } z = H \text{ and } z = 0. \tag{20}$$

The average wall temperatures for the channel top wall (wall a) and channel bottom wall (wall c) are defined as

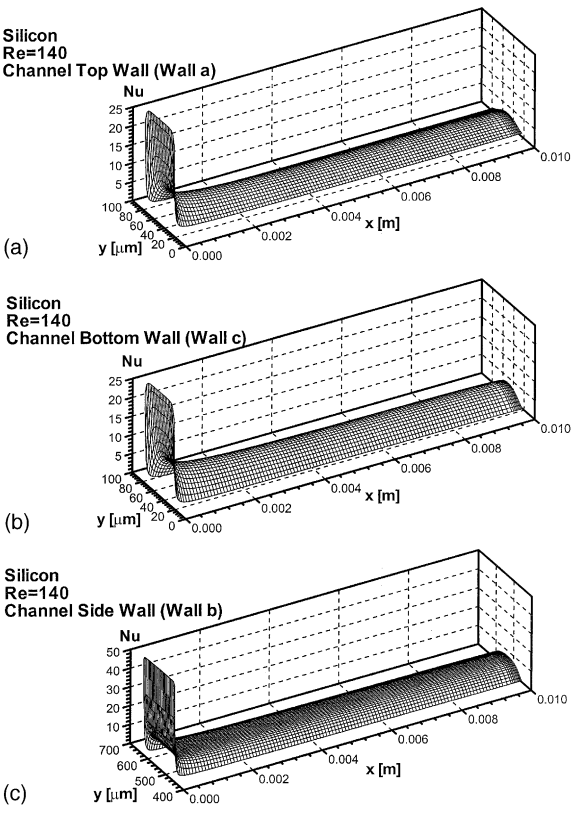

Fig. 9. Local Nusselt number distribution: (a) channel top wall (wall a), (b) channel bottom wall (wall c), (c) channel side wall (wall b).

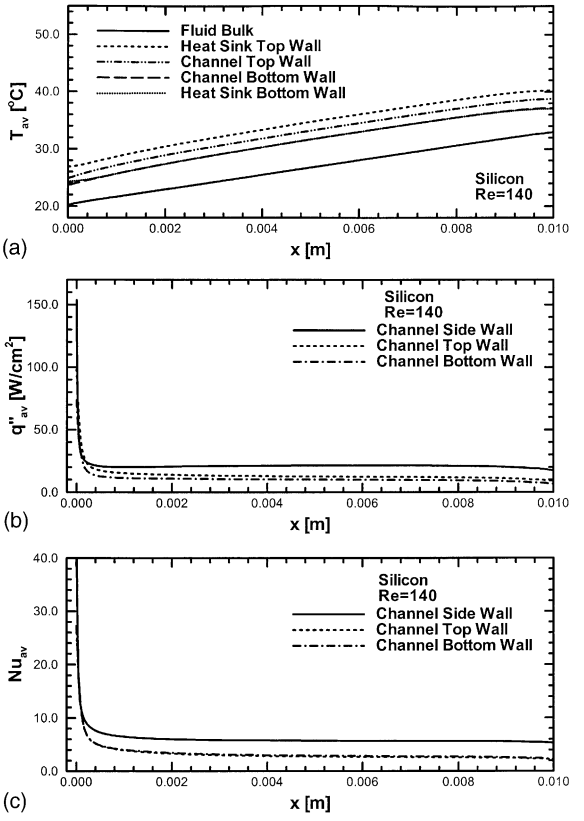

Fig. 10. Average heat transfer characteristics along x-direction: (a) average temperature, (b) average heat flux, (c) average Nusselt number.

$$T_{\mathrm{av}}(x) = \frac{1}{W_{\mathrm{ch}}} \int_{W_{\mathrm{w1}}}^{W_{\mathrm{w1}}+W_{\mathrm{ch}}} T_{\mathrm{s},\Gamma}\,\mathrm{d}y, \quad \text{for } z = H_{\mathrm{w1}} + H_{\mathrm{ch}} \text{ and } z = H_{\mathrm{w1}}. \tag{21}$$

It can be observed that the average temperature decreases from the heat sink top wall to the heat sink bottom wall. The average temperature is nearly the same for the channel bottom wall (wall *c*) and heat sink bottom wall (wall *C*). The liquid bulk temperature is lowest at a given longitudinal distance x. The temperature rise is approximately linear for all the results illustrated. The highest temperature point is located at the heat sink top wall immediately above the channel outlet.

Fig. 10b and c illustrate the average heat flux q''_{av} and average Nusselt number Nu_{av} at the interface between the solid and liquid regions. The definitions of q''_{av} and Nu_{av} at the channel top wall (wall *a*) and channel bottom wall (wall *c*) are similar as the corresponding average wall temperature in Eq. (21). q''_{av} and Nu_{av} at the channel side wall (wall *b*) are defined, respectively, as

$$q''_{\mathrm{av}}(x) = \frac{1}{H_{\mathrm{ch}}} \int_{H_{\mathrm{w1}}}^{H_{\mathrm{w1}}+H_{\mathrm{ch}}} q''\,\mathrm{d}z, \tag{22}$$

$$Nu_{\mathrm{av}}(x) = \frac{1}{H_{\mathrm{ch}}} \int_{H_{\mathrm{w1}}}^{H_{\mathrm{w1}}+H_{\mathrm{ch}}} Nu\,\mathrm{d}z, \tag{23}$$

for $y = W_{\mathrm{w1}}$. Much higher average heat flux and Nusselt number can be found in the region near the channel inlet and decrease rapidly to nearly constant values. The average heat flux at the channel top wall is slightly larger than at the bottom wall, but the corresponding average Nusselt numbers are virtually identical. For most of the channel length, the average heat flux and Nusselt number at the channel top and bottom walls are about half their corresponding values at the channel side wall.

3.3. Effects of Reynolds number

The effects of Reynolds number on the heat transfer process in the micro-channel heat sink are illustrated in Fig. 11a and b for three different Reynolds numbers, 140, 700 and 1400. The fluid inlet temperature and the heat flux supplied to the heat sink top wall are kept constant in the cases studied. Fig. 11a shows the effects on the bulk fluid temperature and the average wall temperature at the heat sink top wall and heat sink bottom wall. It can be seen that the average temperatures decrease with increasing Reynolds number and the differences between the temperature gradients at the channel inlet and outlet are more apparent at high Reynolds numbers.

Fig. 11b shows the effects on the average Nusselt number along the channel top wall and the channel side wall. As Reynolds number increases, a higher average Nusselt number is obtained at a given longitudinal distance x. This trend is maintained even at the channel outlet, which implies the length of the thermal developing region is larger than the channel length. In fact, the fully developed condition may not be achieved inside the heat sink for high Reynolds numbers, even if the gradient of the average Nusselt number near the channel exit is very small.

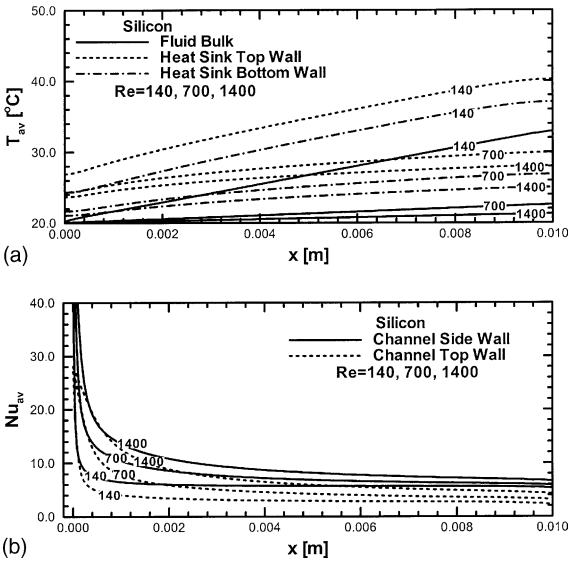

Fig. 11. Effects of Reynolds number on (a) average temperature and (b) average Nusselt number.

3.4. Effects of solid thermal conductivity

The effects of thermal conductivity of solid is explored by substituting copper for silicon as substrate material. The thermal conductivity of copper is about 2.7 times that of silicon as indicated in Table 2. The effects introduced by increasing the solid thermal conductivity are shown in Fig. 12a. It can be seen that changes in the bulk fluid temperature and average temperature at the heat sink bottom wall are very small. However, the average temperature at the heat sink top wall decreases with increasing solid thermal conductivity, especially in the region near the channel outlet.

The average Nusselt number at the channel top wall and the channel side wall for the copper micro-channel heat sink is shown in Fig. 12b. The effects of the solid thermal conductivity on the average Nusselt number are so small that the results for the copper heat sink are virtually identical to those for the silicon heat sink, Fig. 11b.

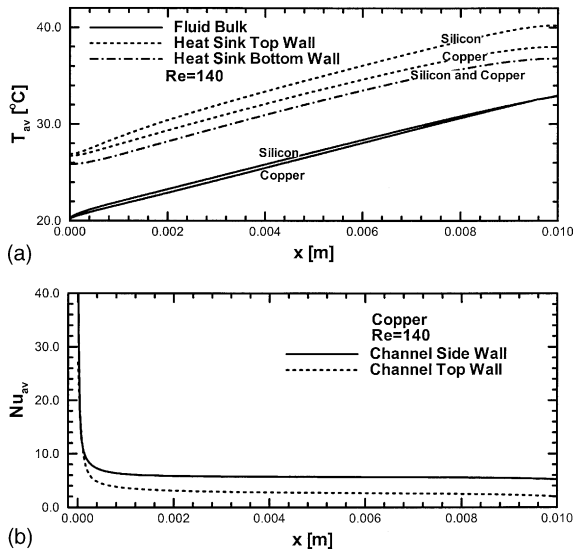

Fig. 12. Effects of thermal conductivity of solid substrate on (a) average temperature and (b) average Nusselt number.

3.5. Assessment of classical fin analysis

One of the major objectives of the theoretical studies is to develop an optimization methodology for the micro-channel heat sink geometry in such a way that the thermal resistance between the heat sink base surface and the cooling fluid is minimized. Several different optimization schemes were developed [3,11,13,14,17]. Unfortunately, very few of those were verified with experiment. As discussed in the previous section, the classical fin analysis is commonly employed in these models. However, this method may not provide accurate results due to the assumptions used and complicated nature of the conjugate heat transfer in the heat sink. In this section, the major approximations introduced in the classical fin analysis method for micro-channel heat sinks operating in the laminar flow regime are summarized and assessed based on the present numerical results.

(1) The solid wall separating two flow channels is approximated in the classical fin analysis as a thin fin and temperature in the wall varies only along the z-direction at each channel cross-section (i.e., each longitudinal distance x). Also at each channel cross-section, the fin-base temperature is uniform and identical to the channel-base temperature. The numerical results of the present study show the temperature in the solid region along the transverse y-direction is nearly constant (Fig. 5a–d), which indicates this assumption is generally valid.

(2) Heat transfer at each heat sink cross-section is modeled in the classical fin analysis as one-dimensional. This assumption is valid in the fully developed region. As shown in Fig. 6a and b, the distribution of constant temperature contour lines along the transverse z-direction is nearly the same for different longitudinal distances x in the fully developed region.

(3) Flow in the channel is assumed laminar and fully developed (hydraulically and thermally) in the classical fin analysis. For low Reynolds numbers, the entrance region is relatively short and the entrance effect is negligible. However, the effects of the developing region become more pronounced at high Reynolds numbers as indicated in Fig. 11b.

(4) The classical fin analysis assumes fluid temperature changes only along the flow direction and is uniform at each channel cross-section (complete thermal mixing). Fig. 6a shows very large temperature gradient exists in the fluid, which clearly disputes the assumption of the classical fin analysis.

(5) The convective heat transfer coefficient along the channel wall is assumed constant and known in the classical fin analysis. This is a poor assumption as shown by the distribution of local Nusselt number in Fig. 9a–c. The convective heat transfer coefficient is a strong function of the channel geometry and local flow condition.

The classical fin method offers the advantages of simplicity and analytical appeal. However, the numerical results of the present study reveal this method can only provide a qualitatively correct picture of heat transport in a micro-channel heat sink.

4. Conclusions

The three-dimensional fluid flow and heat transfer processes in a rectangular silicon micro-channel heat sink were analyzed numerically, and a detailed description of the local and average heat transfer characteristics, i.e. temperature, heat flux, and Nusselt number, was obtained. The effects of Reynolds number and thermal conductivity of the solid substrate on the heat transfer process were discussed. Furthermore, the validity of the major assumptions employed in the classical fin analysis method was investigated based on the numerical results. Key findings from the study are as follows:

(1) The temperature rise along the flow direction in the solid and fluid regions of the micro-channel heat sink can be approximated as linear. The highest temperature point is located at the heated base surface of the heat sink, which is immediately above the channel outlet. The temperature along the transverse

y-direction at a given longitudinal distance x is nearly constant. Also, for a given longitudinal distance x, the temperature gradient along the transverse z-direction in the solid region between the heated heat sink base surface and the flow channel is larger than that in the region between the unheated heat sink base surface and the flow channel.

(2) Much higher heat flux and Nusselt number values are obtained near the channel inlet. The heat flux and Nusselt number also vary around the channel periphery, approaching zero in the corners.

(3) Increasing Reynolds number increases the length of the developing region. Fully developed flow may not be achieved inside the heat sink for high Reynolds numbers. This results in enhanced heat transfer, alas at the expense of a higher pressure drop.

(4) Increasing the thermal conductivity of the solid substrate reduces the temperature of the heated base surface of the heat sink, especially near the channel outlet. The effects on the heat transfer characteristics in the fluid are not significant.

(5) The classical fin analysis method provides a simplified means to modeling heat transfer in micro-channel heat sinks. However, some major assumptions introduced in this method deviate significantly from the real situation. These major assumptions may greatly compromise the accuracy of this method.

Acknowledgements

The authors are grateful for the support from the Office of Basic Energy Sciences of the US Department of Energy (Award no. DE-FG02-93ER14394 A7).

References

[1] I. Mudawar, Assessment of high-heat-flux thermal management schemes, in: Proceedings of the Seventh Intersociety Conference on Thermal and Thermomechanical Phenomena in Electronic Systems, vol. 1, 2000, pp. 1–20.

[2] L.T. Yeh, Review of heat transfer technologies in electronic equipment, ASME J. Electron. Packag. 117 (1995) 333–339.

[3] D.B. Tuckerman, R.F.W. Pease, High-performance heat sinking for VLSI, IEEE Electron. Dev. Lett. EDL-2 (1981) 126–129.

[4] I. Mudawar, M.B. Bowers, Ultra-high critical heat flux (CHF) for subcooled water flow boiling—I: CHF data and parametric effects for small diameter tubes, Int. J. Heat Mass Transfer 42 (1999) 1405–1428.

[5] T. Kishimito, T. Ohsaki, VLSI packaging technique using liquid-cooled channels, IEEE Trans. Components, Hybrids, Manufact. Technol. CHMT-9 (1986) 328–335.

[6] D. Nayak, L.T. Hwang, I. Turlik, A. Reisman, A high performance thermal module for computer packaging, J. Electron. Mater. 16 (1987) 357–364.

[7] M.B. Bowers, I. Mudawar, High flux boiling in low flow rate, low pressure drop mini-channel and micro-channel heat sinks, Int. J. Heat Mass Transfer 37 (1994) 321–332.

[8] T.S. Ravigururajan, J. Cuta, C.E. McDonald, M.K. Drost, Single-phase flow thermal performance characteristics of a parallel micro-channel heat exchanger, National Heat Transfer Conference, vol. 7, ASME HTD-329, 1996, pp. 157–166.

[9] K. Kawano, K. Minakami, H. Iwasaki, M. Ishizuka, Micro channel heat exchanger for cooling electrical equipment, Application of Heat Transfer in Equipment, Systems and Education, ASME HTD-361-3/PID-3, 1998, pp. 173–180.

[10] R.W. Keyes, Heat transfer in forced convection through fins, IEEE Trans. Electron Dev. ED-31 (1984) 1218–1221.

[11] V.K. Samalam, Convective heat transfer in microchannels, J. Electron. Mater. 18 (1989) 611–617.

[12] R.J. Phillips, Micro-channel heat sinks, in: A. Bar-Cohen, A.D. Kraus (Eds.), Advances in Thermal Modeling of Electronic Components, vol. 2, ASME Press, New York, 1990, pp. 109–184.

[13] R.W. Knight, J.S. Goodling, D.J. Hall, Optimal thermal design of forced convection heat sinks-analytical, ASME J. Electron. Packag. 113 (1991) 313–321.

[14] R.W. Knight, D.J. Hall, J.S. Goodling, R.C. Jaeger, Heat sink optimization with application to microchannels, IEEE Trans. Components, Hybrids, Manufact. Technol. 15 (1992) 832–842.

[15] A. Weisberg, H.H. Bau, J.N. Zemel, Analysis of microchannels for integrated cooling, Int. J. Heat Mass Transfer 35 (1992) 2465–2474.

[16] A. Bejan, A.M. Morega, Optimal arrays of pin fins and plate fins in laminar forced convection, ASME J. Heat Transfer 115 (1993) 75–81.

[17] D.Y. Lee, K. Vafai, Comparative analysis of jet impingement and microchannel cooling for high heat flux applications, Int. J. Heat Mass Transfer 42 (1999) 1555–1568.

[18] A.G. Fedorov, R. Viskanta, Three-dimensional conjugate heat transfer in the microchannel heat sink for electronic packaging, Int. J. Heat Mass Transfer 43 (2000) 399–415.

[19] S.B. Choi, R.R. Barron, R.O. Warrington, Fluid flow and heat transfer in micro tubes, ASME DSC 40 (1991) 89–93.

[20] D. Yu, R.O. Warrington, R.R. Barron, T. Ameel, An experimental and theoretical investigation of fluid flow and heat transfer in microtubes, ASME/JSME Therm. Engng. Conf. 1 (1995) 523–530.

[21] X.F. Peng, G.P. Peterson, Convective heat transfer and flow friction for water flow in microchannel structures, Int. J. Heat Mass Transfer 39 (1996) 2599–2608.

[22] T.M. Adams, S.I. Abdel-Khalik, S.M. Jeter, Z.H. Qureshi, An experimental investigation of single-phase forced convection in microchannels, Int. J. Heat Mass Transfer 41 (1998) 851–857.

[23] G.M. Mala, D. Li, Flow characteristics of water in microtubes, Int. J. Heat Fluid Flow 20 (1999) 142–148.

[24] K.C. Pong, C.M. Ho, J. Liu, Y.C. Tai, Non-linear pressure distribution in uniform microchannels, ASME FED 197 (1991) 51–56.

[25] S.V. Patankar, Numerical Heat Transfer and Fluid Flow, Hemisphere, Washington DC, 1980.
[26] S.V. Patankar, A numerical method for conduction in composite materials, flow in irregular geometries and conjugate heat transfer, in: Proceedings of 6th International Heat Transfer Conference, vol. 3, 1978, pp. 297–302.
[27] R.K. Shah, A.L. London, Laminar Flow Forced Convection in Ducts: a Source Book for Compact Heat Exchanger Analytical Data, Supl. 1, Academic Press, New York, 1978.